



HAL
open science

Schumann Resonances as a tool to constrain the depth of Titan's buried water ocean: Re-assessment of Huygens observations and preparation of the EFIELD/Dragonfly experiment

Paul Lagouanelle, Alice Le Gall

► To cite this version:

Paul Lagouanelle, Alice Le Gall. Schumann Resonances as a tool to constrain the depth of Titan's buried water ocean: Re-assessment of Huygens observations and preparation of the EFIELD/Dragonfly experiment. *Icarus*, In press, pp.116372. 10.1016/j.icarus.2024.116372 . insu-04683340v2

HAL Id: insu-04683340

<https://insu.hal.science/insu-04683340v2>

Submitted on 19 Nov 2024 (v2), last revised 15 Dec 2024 (v3)

HAL is a multi-disciplinary open access archive for the deposit and dissemination of scientific research documents, whether they are published or not. The documents may come from teaching and research institutions in France or abroad, or from public or private research centers.

L'archive ouverte pluridisciplinaire **HAL**, est destinée au dépôt et à la diffusion de documents scientifiques de niveau recherche, publiés ou non, émanant des établissements d'enseignement et de recherche français ou étrangers, des laboratoires publics ou privés.

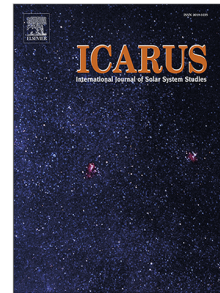


Distributed under a Creative Commons Attribution 4.0 International License

Journal Pre-proof

Schumann Resonances as a tool to constrain the depth of Titan's buried water ocean: Re-assessment of Huygens observations and preparation of the EFIELD/Dragonfly experiment

Paul Lagouanelle, Alice Le Gall



PII: S0019-1035(24)00432-9
DOI: <https://doi.org/10.1016/j.icarus.2024.116372>
Reference: YICAR 116372

To appear in: *Icarus*

Received date: 31 July 2024

Revised date: 4 November 2024

Accepted date: 8 November 2024

Please cite this article as: P. Lagouanelle and A. Le Gall, Schumann Resonances as a tool to constrain the depth of Titan's buried water ocean: Re-assessment of Huygens observations and preparation of the EFIELD/Dragonfly experiment. *Icarus* (2024), doi: <https://doi.org/10.1016/j.icarus.2024.116372>.

This is a PDF file of an article that has undergone enhancements after acceptance, such as the addition of a cover page and metadata, and formatting for readability, but it is not yet the definitive version of record. This version will undergo additional copyediting, typesetting and review before it is published in its final form, but we are providing this version to give early visibility of the article. Please note that, during the production process, errors may be discovered which could affect the content, and all legal disclaimers that apply to the journal pertain.

© 2024 Published by Elsevier Inc.

Revised Manuscript

Highlights

Schumann Resonances as a tool to constrain the depth of Titan's buried water ocean: Re-assessment of Huygens observations and preparation of the EFIELD/Dragonfly experiment

Paul Lagouanelle, Alice Le Gall

- Surrogate modeling of Titan's planetary cavity for Schumann resonances
- Re-assessment of Huygens observations to constrain the thickness of Titan's ice crust
- Potential performances of the EFIELD experiment on board Dragonfly for estimating the thickness of the ice crust

Schumann Resonances as a tool to constrain the depth of Titan's buried water ocean: Re-assessment of Huygens observations and preparation of the EFIELD/Dragonfly experiment

Paul Lagouanelle^a, Alice Le Gall^a

^aLATMOS/IPSL, Université Paris-Saclay, UVSQ, Sorbonne Université, CNRS, 78280, Guyancourt, France

ARTICLE INFO

Keywords:

Titan, interior
Instrumentation
Ionospheres
Radio observations
Titan, atmosphere

ABSTRACT

Among the lines of evidence for a buried ocean on Titan is the possible detection of Schumann-like Resonances (SR), in 2005, by the Permittivity, Wave and Altimetry (PWA) analyzer on board the ESA Huygens probe. SR are Extremely Low Frequency electromagnetic waves resonating between two electrically conductive layers. On Titan, it has been proposed that they propagate between the moon's ionosphere and a salty subsurface water ocean. Their characterization by electric field sensors can provide constraints on Titan's cavity characteristics and in particular on the depth of Titan's ocean which is key to better assess Titan's habitability. For this work we have developed a numerical model of Titan's electromagnetic cavity as well as a surrogate model (i.e., an approximate mathematical model) able to accurately approximate the behavior of the cavity. This surrogate model can be used to conduct simulations and sensitivity analyses at a low computational cost. It is used both to re-assess PWA/Huygens measurements and to predict the future performance of the EFIELD experiment on board the NASA Dragonfly mission. We demonstrate that the PWA/Huygens measurements, in particular due to their low spectral resolution, do not bring any meaningful constraint on Titan's ocean depth. On the other hand, the finer resolution of the EFIELD experiment and its ability to capture several harmonics of SR should provide more robust constraints on Titan's internal structure, especially if the electrical properties of the ice crust and the atmosphere can be better constrained.

1. Introduction

Several lines of evidence point to the presence of a global water ice ocean in Titan's interior. The strongest evidence arises from the investigation of the tidal variations of Titan's gravity fields inferred from Cassini flybys of the satellite (Jess et al., 2012; Durante et al., 2019). Indeed, the tidal Love number k_2 of 0.62 derived by Durante et al. (2019) is compatible with a high-density ocean while a recent re-assessment of k_2 (0.375) points to a low-density water or ammonia ocean (Goossens et al., 2024). Titan's measured obliquity of $\sim 0.3^\circ$ (Stiles et al., 2008; Meriggiola et al., 2016) is also significantly larger than the value expected for an entirely solid object and therefore suggests a decoupling between the outer ice shell and the interior of Titan (Baland et al., 2011, 2014; Bills and Nimmo, 2008, 2011). Based on both the values of Durante et al. (2019)'s k_2 and of the obliquity, Baland et al. (2014) estimate that the outer ice shell of Titan is at least 40 km and at most 170 km thick consistent with the results published in Kronrod et al. (2020) which test a wide range of internal structure models for Titan including thermal considerations.

Another, possible evidence for an internal ocean on Titan is the detection of ELF (Extremely Low Frequency) waves by the PWA/HASI (Permittivity, Waves and Altimetry analyzer, part of the Huygens Atmospheric Structure Instrument) experiment on board the Huygens interpreted as Schumann Resonances (Béghin et al., 2012). Schumann resonances (SR) are a set of ELF (from a few Hz up to 100 Hz) electromagnetic propagation modes that can develop in a planetary cavity excited by a broadband electromagnetic source (Schumann, 1952). On Earth, these modes are generated by lightning discharges and propagate between the ionosphere and the surface. Theoretically, SR could be observed on other planets and serve as a tool to obtain information on the planetary cavities, in particular on their dimensions (Simoes, 2007; Simões et al., 2008a,b).

If SR exist on Titan, they are probably not triggered by lightning as such activity is not expected to be common on Titan (Lorenz, 1997) and was never observed during the Cassini mission, nor by the Radio and Plasma Wave Science (RPWS) experiment (Fischer et al., 2007, 2020; Fischer and Gurnett, 2011) nor by PWA/HASI (Hamelin et al., 2009). In addition, the surface of Titan being very poorly conductive (Grard et al., 2006; Hamelin et al., 2016), it cannot act

ORCID(s):

24 as the lower boundary of the resonant cavity which instead must be an internal electrically conductive layer. Béghin
 25 et al. (2012) propose that SR on Titan could be excited by interactions with Saturn's magnetosphere and that the
 26 signal detected at ~ 36 Hz by PWA/HASI is the second harmonic of a SR propagating between Titan's fully ionized
 27 atmospheric layer (at $\sim 60 - 70$ km altitude) and a buried salty ocean lying at a depth encompassed between 40 and
 28 80 km. However, this interpretation is still debated as the 36 Hz line may actually be due to mechanical oscillations
 29 of the booms on which the PWA/HASI electrodes were installed or of other parts of the Huygens probe (Lorenz and
 30 Le Gall, 2020).

31 Nevertheless, if SR occur on Titan, their detection and characterization would place new and more robust
 32 constraints on the buried ocean. In particular, knowing more accurately its depth is key to estimate the likeliness of
 33 exchange between the ocean and the surface and therefore to assess Titan's habitability and astrobiological potential.
 34 That is the reason why the forthcoming mission to Titan, Dragonfly (NASA), will embark sensors to measure the
 35 time-varying electrical field, namely the EFIELD experiment which is part of the DraGMet (Dragonfly Geophysics
 36 and Meteorology) package (Barnes et al., 2021). Using two spherical electrodes mounted at different locations on the
 37 body of the Dragonfly drone, EFIELD will passively record the AC electrical field between ~ 5 and 100 Hz with a
 38 much finer spectral resolution than PWA/HASI.

39 In this paper, we describe the numerical model we have developed to simulate Titan's electromagnetic cavity
 40 and predict its resonant frequencies and associated quality factors (section 2). This model is used to build a much
 41 less computationally expensive surrogate model which allows to perform an accurate sensitivity analysis of the SR
 42 characteristics to the cavity parameters. The surrogate model is then used to re-examine the PWA/HASI measurements
 43 leading to results very different from the ones published in Béghin et al. (2012) (section 3). In section 4, it is used
 44 to investigate the expected performance of the EFIELD/DraGMet experiment. Lastly, we conclude and discuss the
 45 implications of this work in section 5.

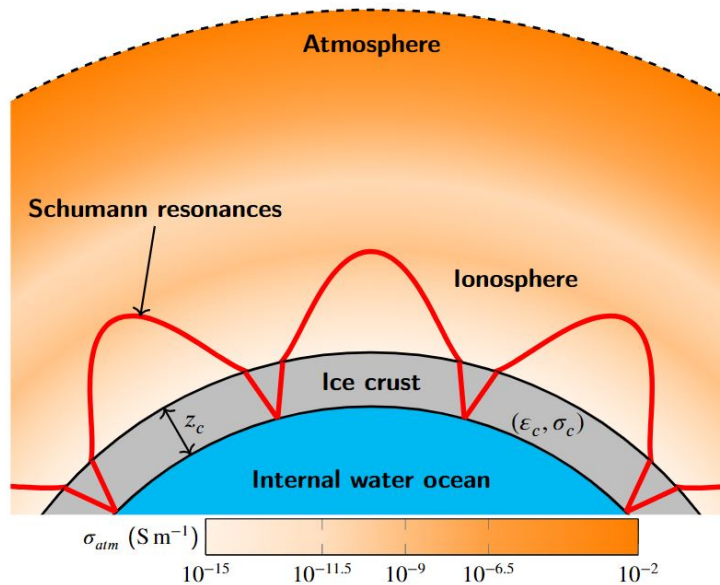


Figure 1: Structure and parameters of Titan's cavity

46 2. Modeling Titan's resonant cavity

47 Following Simões et al. (2007, 2008a,b) who developed cavity models for Titan, Venus and other planetary
 48 environments, we used the COMSOL Multiphysics© tool to build a numerical model of electromagnetic wave

49 propagation in the cavity of Titan. We then used the numerical model to construct a surrogate model of the propagation
50 of SR on Titan in order to conduct eigenfrequency analysis at a low computing and memory cost.

51 2.1. Numerical model

52 2.1.1. Cavity description and parameters

53 The numerical code solves the Maxwell's equations in a spherical structure made of discrete slabs. Figure 1 displays
54 the simplified structure of Titan's cavity we considered; it consists of three concentric layers:

- 55 • *the atmosphere/ionosphere layer* for which an analytic conductivity profile is given to the model, namely the one
56 proposed by Béghin et al. (2012) or, more recently, by Lorenz (2021) displayed in figure 2. Both conductivity
57 models include a fully ionized layer at an altitude of about 60–70 km on which ELF waves are reflected. They rely
58 on Huygens measurements of the electron-density performed from an altitude of 140 km down to the surface
59 (Grard et al., 2006). In Lorenz (2021), the conductivity profile is interpolated from 140 to 750 km and better
60 respect the upper limit of the near-surface conductivity imposed by Huygens Relaxation Probe measurements.
- 61 • *the ice crust layer* in which ELF waves are refracted following Fresnel's laws. This layer is assumed uniform in
62 terms of electrical properties with a very small conductivity that allows ELF waves to propagate over a very
63 long path (i.e., the skin depth is > 1000 km).
- 64 • *the salty ocean layer* which is assumed to be a perfect electric conductor and therefore on which ELF waves are
65 fully reflected.

66 The parameters of the cavity model considered for parametric analysis are the followings:

- 67 • *the thickness of the ice crust z_c* : Based on Cassini and Huygens observations as well as on gravity and thermal
68 modeling (see section 1), we consider that z_c can vary over a wide range of values from 5 to 200 km, and most
69 likely between 40 and 170 km.
- 70 • *the real part of the ice crust relative permittivity ϵ_c* : The relative permittivity of water ice at Titan's temperatures
71 and ELF frequencies is ~ 3 (e.g., Mattei et al. (2014)). However, the crust permittivity also depends on its
72 porosity and on the presence of impurities or contaminants such as ammonia. We therefore test values in the
73 range 2 – 4 which encompasses the value measured at the Huygens landing site by the permittivity probe
74 PWA-MIP/HASI, namely 2.5 ± 0.3 (Hamelin et al., 2016).
- 75 • *the electrical conductivity of the ice crust σ_c* : Through expected to be small, the conductivity of the ice crust of
76 Titan remains uncertain. It is especially sensitive to the possible presence of ionic contaminants. Béghin et al.
77 (2012) investigates the $1 - 4$ nS m⁻¹ range while Hamelin et al. (2016) found a conductivity of 1.2 ± 0.6 nS m⁻¹
78 at the Huygens landing site. To account for this measurement, we consider values in the range $0.6 - 4$ nS m⁻¹.

79 As outputs, the numerical model computes the eigenfrequencies of the first three modes of the resonant cavity
80 (f_1, f_2, f_3) along with their corresponding Q-factors (quality factors: Q_1, Q_2, Q_3) which describe wave attenuation in
81 the cavity. More specifically, the model provides the complex frequencies of the different eigenmodes from which the
82 Q-factor is computed as followed:

$$83 Q_n = \frac{\text{Re}(f_n)}{2\text{Im}(f_n)} \approx \frac{f_n}{\Delta f_n} \quad (1)$$

84 where Re and Im are respectively the real and imaginary parts of the complex eigenfrequency, f_n is the peak power
85 frequency of mode n , and Δf_n is the width at half-power.

86 For a given uncertainty δf_n on f_n and Δf_n , which in practice is mainly dictated by the measurement spectral
87 resolution, the uncertainty δQ_n on the corresponding quality factor Q_n can be derived by logarithmic differentiation
of equation 1:

$$\delta Q_n \approx Q_n(1 + Q_n) \frac{\delta f_n}{f_n} \quad (2)$$

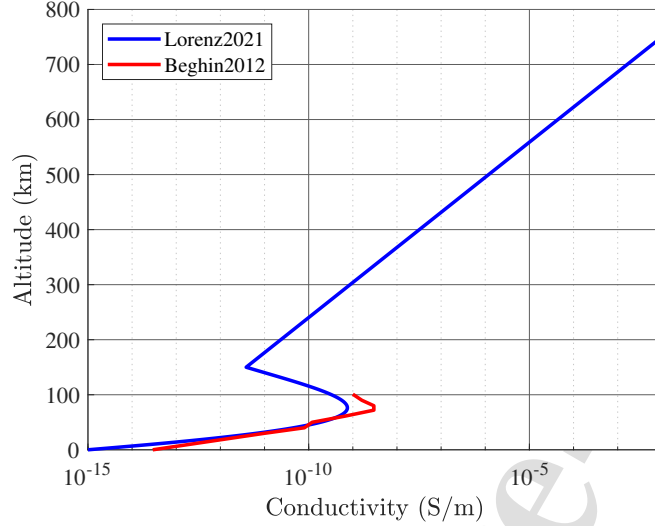


Figure 2: Input conductivity profiles of the atmosphere/ionosphere layer used in the numerical model of Titan's cavity from Béghin et al. (2012) (red) and Lorenz (2021) (blue)

Table 1

Comparison of results with the 2D axi-symmetric approximation model with the 3D model for two different cavities (and associate relative error)

Model	Q_1	$\Delta Q_1/Q_1$	f_1	$\Delta f_1/f_1$	Q_1	$\Delta Q_1/Q_1$	f_1	$\Delta f_1/f_1$
2D axi-symmetric	3.20	4.69%	32.61 Hz	0.797%	2.735	2.93%	18.28 Hz	1.70%
3D	3.05	4.92%	32.35 Hz	0.803%	2.655	3.01%	17.97 Hz	1.73%

(a) First case: $z_c = 20$ km, $\epsilon_c = 3.94$, $\sigma_c = 9.69 \times 10^{-9}$ S m $^{-1}$

(b) Second case: $z_c = 15$ km, $\epsilon_c = 2.5$, $\sigma_c = 1 \times 10^{-9}$ S m $^{-1}$

Table 2

Comparison of results with the 2D axi-symmetric approximation model with the model used in Simoes (2007) (relative error ϵ)

Model	f_1	$\Delta f_1/f_1$	f_2	$\Delta f_2/f_2$	f_3	$\Delta f_3/f_3$
2D axi-symmetric	22.54 Hz	1.06%	39.08 Hz	1.20%	55.27 Hz	1.23%
Simoes (2007)	22.30 Hz	1.08%	38.61 Hz	1.22%	54.59 Hz	1.25%

2.1.2. Numerical approach

The numerical model uses the Finite Element Method (Zimmerman, 2006) for solving Maxwell's equations with the boundary conditions and layers properties as described above. Since layers properties are only functions of the radial distance, the resonant cavity problem can be solved in a 2D axi-symmetric configuration. We nevertheless validate our 2D model with comparison to a 3D model and results from the numerical model from Simoes (2007).

An example of a 3D model of Titan's cavity is displayed on figure 3 as well as a 2D cut of the mesh. Due to the level of discretization needed to accurately reproduce the behavior of the electric field in Titan's atmosphere, the complete 3D mesh consists of 774,258 domain elements, 181,100 boundary elements, and 2,588 edge elements. A single resolution of Maxwell's equations using such a mesh takes ~ 2 h (on an Intel Core i5-12500H, 2.5 GHz, 32 GB of RAM). In contrast, the design of a 2D axi-symmetric model with a mesh composed of 202,993 domain elements

and 3,652 boundary elements requires ~ 30 s of computation time which is much more reasonable for the purpose of using the model to perform an accurate parametric inversion.

Table 1 reports the results from the 3D model and the 2D approximation for two different cavities. The 2D approximation is accurate enough so that the results from the 3D model are reproduced with relative errors smaller than 5% for both the Q-factor and the resonant frequency. Table 2 reports the results from the 2D approximation and the model from Simoes (2007) showing that the 2D approximation is able to accurately reproduce the cavity behavior in the case of study case with a relative error on the first three resonant frequencies smaller than 2%. Thus, for the remainder of the paper, we only consider the 2D axi-symmetrical model of Titan's planetary cavity.

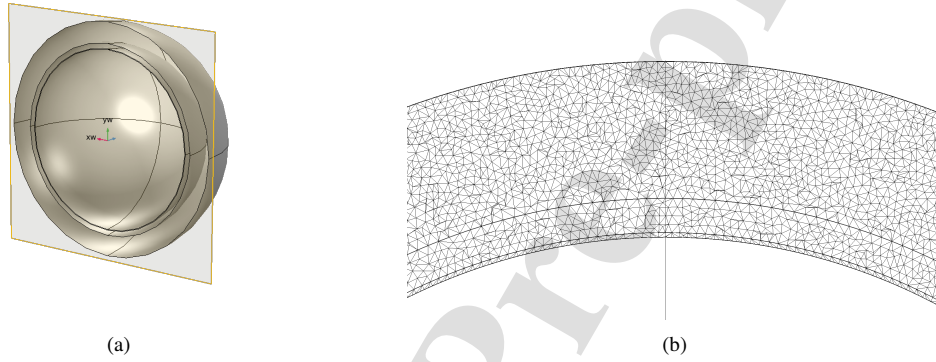


Figure 3: (a) 3D model of Titan's planetary cavity on COMSOL Multiphysics, (b) 2D cut of the 3D mesh on (a).

2.2. Surrogate model

Even with the 2D axi-symmetrical approximation, a complete sensitivity analysis or data inversion using Titan's cavity numerical model would require to compute several thousand of datapoints. This would represent a significant amount of computation time that is not suitable even for a supercomputer. To avoid this, we built a surrogate model (also called "metamodel") which provides an approximate description of the behavior of Titan's resonant cavity by analytical functions. The resulting metamodel can then be used, instead of the numerical model, to perform various analysis (e.g. optimization, sensitivity analysis) at a low computational cost (Van Steenkiste et al., 2016).

2.2.1. Description

The surrogate model used here is an exact interpolator; the Polynomial-Chaos based Kriging (PCK) (Schobi et al., 2015) metamodeling combines both Polynomial Chaos Expansion (PCE) and Kriging to predict the variations of a given model $\mathcal{M}(X)$. Kriging is used to interpolate the local variations of the output model while PCE is useful for the global approximation. A PCK metamodel is defined by:

$$\mathcal{M}(X) = \sum_{\alpha \in \mathcal{A}} y_{\alpha} \psi_{\alpha}(X) + \sigma^2 Z(X, \omega) \quad (3)$$

where $\sum_{\alpha \in \mathcal{A}} y_{\alpha} \psi_{\alpha}(X)$ is a weighted sum of orthonormal polynomials describing the trend of the PCK model and $\sigma^2 Z(X, \omega)$ is a zero-mean stationary Gaussian process with a variance of σ^2 . The computation of the metamodel parameters is performed by the UQLab framework available on Matlab (Marelli and Sudret, 2014).

The costly part of the metamodeling process is the training time which can be greatly reduced by using sequential sampling instead of classical space-filling approaches. In this work an adaptive sampling algorithm combined with PCK has been used to build the metamodel. This algorithm has already been proven useful for various electromagnetic problems (Lagouanelle et al., 2023).

2.2.2. Metamodel accuracy

Once built, the surrogate model is used to predict the behavior of the cavity outside of the training data. For such a purpose, a proper metric is crucial to quantify the accuracy of these predictions. A classical approach consists in using

128 a validation dataset outside of the training dataset and computing the mean squared error (MSE) of the metamodel
 129 prediction compared to the real input values. However, the resulting MSE is biased by the use of only one dataset
 130 and could vary greatly from one validation dataset to another. Moreover, this approach requires additional calls of the
 131 expensive computational numerical model for building the training dataset, which ultimately increases the computation
 132 time. Thus, a better metric was chosen : the Leave-one-out cross-validation error (*LOO*), which does not require
 133 additional computations.

134 Let us consider a set $\{(X_1, Y_1), \dots, (X_N, Y_N)\}$ of N input samples. Using this set, one can build a PCK metamodel
 135 \mathcal{M} and evaluate the *LOO* as follows:

$$LOO = \frac{1}{N} \sum_{i=1}^N \left(\frac{\|\mathcal{M}_{/i}(X_i) - Y_i\|}{\|Y_i\|} \right)^2 \quad (4)$$

136 where $\mathcal{M}_{/i}$ is the mean predictor that was trained using all (X, Y) except (X_i, Y_i) . For a given datapoint (X_i, Y_i) , a
 137 metamodel is built with all datapoints except datapoint i , which gives $N - 1$ training datapoints. This metamodel
 138 is then used to predict the value Y_i at the remaining datapoint i , where the difference is classified with a MSE. The
 139 process is repeated for every datapoint which, after average, provides the *LOO*. The use of N different validation
 140 sets of one datapoint guarantees that the *LOO* is much less biased than a classical MSE and reduces the probability of
 141 overestimating the validation error (Elisseeff et al., 2003). In this work, we therefore consider the *LOO* as our accuracy
 142 metric. A *LOO* close to 1 (or 100%) implies that the surrogate model does not provide a good approximation of the
 143 system. On the other hand, the smaller the *LOO*, the more accurate the surrogate model.

144 2.2.3. Sensitivity indices

145 Since the resulting metamodel consists of an analytical function, calling the metamodel is extremely cheap in
 146 terms of computation time. Thus, sensitivity analyses, which are usually performed by Monte-Carlo analyses over the
 147 parameter spaces, are now feasible at a low computation cost.

148 The sensitivity analysis we conduct relies on Sobol' indices which are scalars between 0 and 1 describing the
 149 influence of a set of inputs on a model output (Sobol, 1993). The most commonly used Sobol' indices is the first-order
 150 Sobol' index defined, for a given parameter P_i , as:

$$S_i = \frac{\text{Var}_{P_i}(\mathbb{E}_{X_{/i}}(Y|X_i))}{\text{Var}(Y)} \quad (5)$$

151 S_i is a measure of the fraction of the output variance caused by the variance of a given input parameter. In other words,
 152 it describes the impact of a parameter P_i alone on the output model compared to other parameters. The closer to 1, the
 153 bigger impact P_i has on the model output.

154 However, parameters are usually not independent and their relative effects cannot be separated from each other.
 155 This leads to the definition of higher-order Sobol' indices as, for a subset of parameters $(P_{i_1}, \dots, P_{i_s})$:

$$S_{i_1, \dots, i_s} = \frac{\text{Var}_{(P_{i_1}, \dots, P_{i_s})}(\mathbb{E}_{X_{/i_1, \dots, i_s}}(Y|X_{i_1}, \dots, X_{i_s}))}{\text{Var}(Y)} \quad (6)$$

156 which describes the sensitivity of the model to the variations of several input parameters simultaneously.

157 For high dimensional output models, the interpretation of all orders Sobol' indices can be difficult due to the high
 158 number of possible combinations. Therefore, for an input parameter P_i , a total-effect index (or total Sobol' index) S_i^T
 159 is defined by summing all the Sobol' indices as follows:

$$S_i^T = \sum_{\{u, u \subseteq [1, d] \text{ and } i \in u\}} S_u \quad (7)$$

160 S_i^T is the most suited sensitivity tracker for our study and will be referred to as S_i in the remainder of the paper. When
 161 using PCK metamodels, the computation of the various Sobol' indices of the surrogate model can be easily extracted
 162 from the polynomial decomposition (see equation 3). Therefore, no additional computation of the surrogate model are
 163 required to perform the sensitivity analysis based on the total Sobol' indices.

3. Re-assessment of PWA/HASI/Huygens observations

Fulchignoni et al. (2005) first reported the detection of a narrow spectral feature at ~ 36 Hz in the ELF spectrum measured by PWA/HASI during Huygens' descent in Titan's atmosphere in January 2005, from an altitude of 140 km down to the surface. The magnitude of this signal is especially enhanced just after the deployment of the stabilizer parachute, at an altitude of ~ 110 km. Béghin et al. (2007) proposed different scenarios, both natural and artificial, to explain the 36 Hz signal. In Béghin et al. (2012), a natural scenario is preferred: the signal and associated Q-factor of about ~ 6 would be the second harmonic of a SR propagating between Titan's ionosphere and ocean and triggered by interactions with Saturn's magnetosphere. Using an approximate analytical model of Titan's cavity, Béghin et al. (2012) further derive constraints on the physical parameters of the cavity from PWA/HASI measurements. More specifically, they conclude that the measured $f_2 = 36 \pm 3$ Hz and $Q_2 \sim 6$ are indicative of a water-ammonia ocean lying at a depth of 40 – 80 km.

In this section, we re-assess the PWA/HASI data using the surrogate model we have developed (see section 2) to investigate, in a more accurate fashion, the constraints Huygens measurements bring on the thickness of the ice crust (i.e., the depth of the ocean) z_c . As a starting point, we adopt exactly the same hypotheses as in Béghin et al. (2012) that is the same conductivity profile in the atmosphere and ranges of variation for ϵ_c (2 – 4) and σ_c (1 – 4 nS m⁻¹).

The metamodeling process estimates consistently ($LOO \approx 3.9\%$, $n_{samples} = 1584$) the second harmonic of SR (f_2 , Q_2). Using the resulting surrogate model, two regular 3D grids of f_2 and Q_2 values along all three input parameters z_c , ϵ_c and σ_c can be computed at a low computation cost: $50 \times 50 \times 50 = 125,000$ values, which would have taken 43 days of computation time using directly the numerical model instead of only 13 hours for training the metamodel.

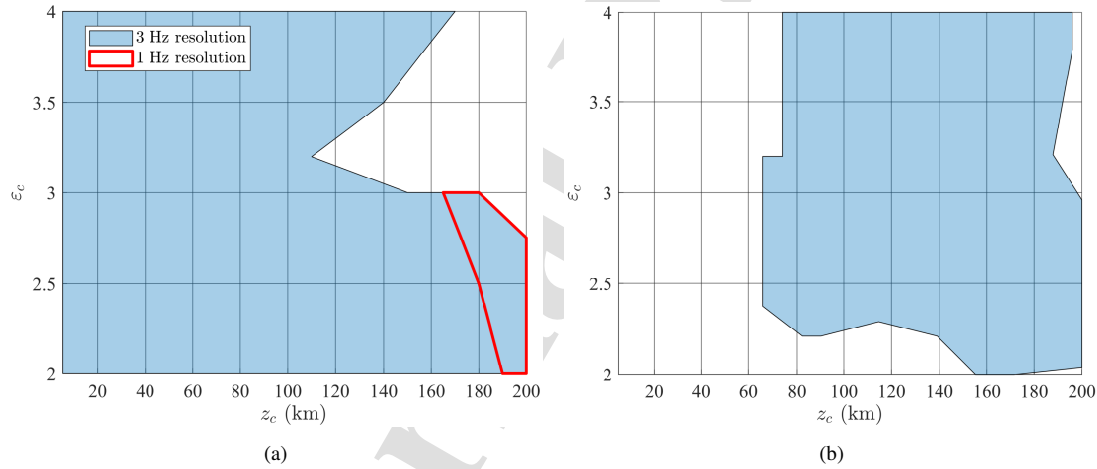


Figure 4: Inversion of Huygens PWA/HASI data taking the same hypotheses as in Béghin et al. (2012) (i.e., conductivity profile, $\epsilon_c \in [2 - 4]$ and $\sigma_c \in [1 - 4]$ nS m⁻¹) and using the surrogate model developed in this work (a). All values of z_c can be in a combination with ϵ_c and σ_c that reproduces Huygens data which were measured with a 3 Hz spectral resolution. A 1 Hz spectral resolution would drastically reduce the parameter space for z_c . (b) displays the same inversion exercise but considering that the detected line at 36 Hz is the fundamental of the SR instead of the second harmonic (no inversion solution for a 1 Hz spectral resolution in this case).

By analyzing the 3D grids, every combination of z_c , ϵ_c and σ_c which gives $f_2 \in [33 - 39]$ Hz and $Q_2 \in [3 - 9]$ can be classified as a potential solution explaining Huygens measurements. Figure 4a displays all the potential inversion of Huygens measurements in the plane (z_c , ϵ_c) where all the grids in the direction σ_c have been stacked. When accounting for 3 Hz spectral resolution, the range of possible values for z_c covers all the parameter space (i.e. 5 – 200 km) which means that no constraint can be deduced on z_c from the PWA/HASI dataset (blue zone). On the other hand, if the signal characteristics were known with a 1 Hz resolution, only a narrow range of z_c values could explain the observations (red outlined area). This hypothetical inversion would restrain the thickness of the ice crust to $z_c \in [165 - 200]$ km.

190 Our results are in contradiction with Béghin et al. (2012) which can be explained by the various analytical
 191 approximations they consider to solve the wave propagation equation. Furthermore, since the metamodel is sufficiently
 192 accurate ($LOO \approx 3.9\%$), it can be used to conduct an accurate Sobol'-based sensitivity analysis. The following total
 193 Sobol' indices are found: $S_{z_c} = 0.73$, $S_{\epsilon_c} = 0.28$ and $S_{\sigma_c} = 0.74$. These indexes indicate that the ice crust thickness
 194 is the parameter that has the most significant impact on the SR characteristics. However, since all indexes are of the
 195 same order of magnitude, no parameter can be regarded as having a negligible impact. This is a further guarantee that
 196 the metamodel accuracy is correctly estimated with the LOO and that our metamodel is highly accurate. Therefore the
 197 differences from Béghin et al. (2012)'s results and the present work cannot be ascribed to an incorrect estimate of the
 198 errors from the metamodel.

199 The surrogate model also demonstrates that solutions (in terms of combinations of z_c , ϵ_c and σ_c values) in which
 200 the detected signal is not the second harmonic but the fundamental are possible (figure 4b). If so, the constraints on z_c
 201 derived from PWA/HASI would be different (namely >80 km, see figure 4b).

202 Lastly, figure 5 shows how the constraints on z_c are modified if the numerical model from which the surrogate
 203 model was built rather uses Lorenz (2021)'s conductivity profile and values of ϵ_c and σ_c from Hamelin et al. (2016).
 204 We will keep these hypotheses for the remainder of the paper and, in particular, to assess EFIELD/DraGMet future
 205 performance in the frame of the Dragonfly mission. The associated sensitivity analysis provides the following total
 206 Sobol' indices: $S_{z_c} = 0.78$, $S_{\epsilon_c} = 0.34$ and $S_{\sigma_c} = 0.51$. Again and notably, z_c is the parameter that have the most
 207 impact on SR characteristics. Nevertheless, the effects of ϵ_c and σ_c cannot be neglected as their respective total Sobol'
 208 index are of the same order of magnitude. This further implies that their accurate knowledge would greatly reduce the
 209 uncertainty on the inversion of Huygens measurements as well as be very valuable for the analysis of future EFIELD
 210 data. In particular, if the real part of the permittivity of the ice crust were measured as $\epsilon_c = 2.5 \pm 0.1$ instead of 2.5 ± 0.3 ,
 211 it would help discriminating between the two distinctive domains in figure 5: $z_c \in [5-40]$ km and $z_c \in [150-200]$ km.
 212 This is further discussed below.

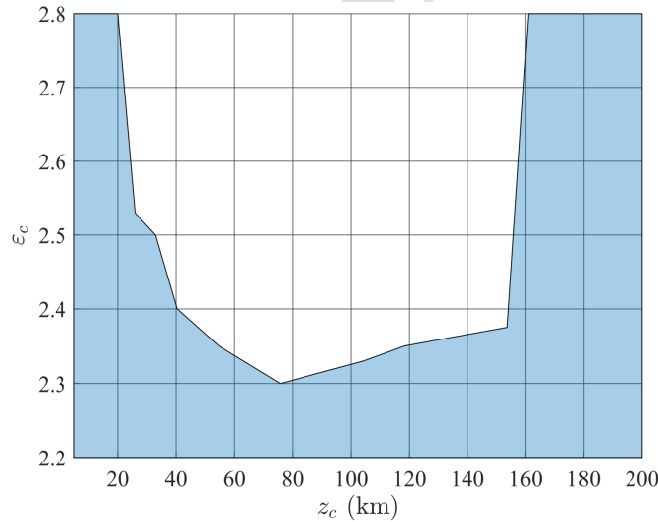


Figure 5: Inversion of Huygens PWA/HASI using the surrogate model developed in this work with up-to-date assumptions, namely the atmosphere conductivity profile from Lorenz (2021) and $\epsilon_c \in [2.2-2.8]$ and $\sigma_c \in [0.6-1.8]$ nS m⁻¹ as estimated by Hamelin et al. (2016).

213 4. Anticipated EFIELD/DraGMet/Dragonfly performance

214 This section investigates the performance and possible outcome from the forthcoming electric-field experiment on
 215 Titan.

4.1. The EFIELD experiment on board Dragonfly

In June 2019, NASA selected the Dragonfly mission project for its New Frontiers program (Turtle et al., 2018; Lorenz et al., 2018; Barnes et al., 2021). The primary goal of the Dragonfly mission is to investigate the chemistry and habitability of Titan. Starting operations in mid-2030s, the Dragonfly quadcopter drone will visit a variety of sites, from a dune field to the rim of a young impact crater, and sample materials in different geologic settings. Dragonfly includes a Geophysical and Meteorological package (DraGMet) which is a suite of sensors designed to measure e.g. the temperature, pressure, methane humidity, wind speed and direction, ground dielectric constant, thermal properties and level of seismic activity at each Dragonfly landing site.

Among these sensors is the EFIELD experiment which consists of two independent spherical electrodes (~ 5 cm in diameter) accommodated at the end of ~ 25 cm long stalks pointing away from the drone body. From two different locations on the drone, these electrodes will passively record the time-varying electrical field at low frequencies ($\sim 5 - 100$ Hz) with the main goal of detecting SR, if any. As a secondary objective, the EFIELD probes will detect and characterize near-surface wind-blown charged grains flying in their vicinity (Chatain et al., 2023).

The EFIELD experiment offer many advantages over the PWA/HASI one. It will operate during an extended period of time (several times a Titan day for the 3.3 years of the nominal mission), from a stable and much mechanically-quieter platform than the Huygens probe. Further, the EFIELD design should guarantee a spectral resolution of 1 Hz (against, at best, 3 Hz for PWA/HASI) and the capture of the first three harmonics of the SR. Figure 4a demonstrates how valuable a finer spectral resolution would be to bring more robust constraints on the depth of the buried ocean z_c . The benefit of detecting more than one SR harmonics is investigated below.

4.2. Multi-modal analysis

The re-assessment of Huygens data presented in section 3 relies on the measurement of only one mode of the SR; it concludes that a wide range of values are possible for the thickness of the ice crust ($z_c \in [5 - 200]$ km). The multi-modal analysis of SR enabled by EFIELD should drastically reduce this range because, in addition to a better spectral resolution, the three first modes of the Schumann resonances will be associated with three different domains of possible z_c values whose intersection may be narrow.

As an illustration, we numerically simulate Titan's cavity for the following parameter values: $z_c = 60$ km, $\epsilon_c = 2.5$, $\sigma_c = 1.2$ nS m $^{-1}$ and the up-to-date conductivity profile from Lorenz (2021). The numerical model provides the following outputs: $f_1 = 28.4$ Hz, $f_2 = 44.9$ Hz, $f_3 = 62.4$ Hz along with their corresponding quality factors: $Q_1 = 3.25$, $Q_2 = 3.58$ and $Q_3 = 3.81$. Using the metamodel, we further compute the variations of the resonant frequencies (f_1, f_2, f_3) and of the quality factors (Q_1, Q_2, Q_3) as a function of the thickness of the ice crust z_c , assuming fixed values for $\epsilon_c = 2.5$ and $\sigma_c = 1.2$ nS m $^{-1}$. These variations are displayed on figure 6.

Assuming a 1 Hz resolution, each harmonic can be inverted separately (using the method described in section 3), resulting in three different possible domains for z_c :

- $f_1 = 28.4 \pm 1$ Hz $\implies z_c \in [19.7 - 21.3] \cup [56.0 - 73.0] \cup [81.4 - 85.8]$ km
- $f_2 = 44.9 \pm 1$ Hz $\implies z_c \in [20.9 - 22.4] \cup [54.8 - 72.3] \cup [83.4 - 87.8]$ km
- $f_3 = 62.4 \pm 1$ Hz $\implies z_c \in [21.7 - 23.5] \cup [33.2 - 46.3] \cup [56.7 - 63.2]$ km

The intersection of these domains is: $z_c \in [56.7 - 63.2]$ km which corresponds to an uncertainty of 6% with respect to the input value of 60 km. A similar inversion is performed on the quality factors separately:

- $Q_1 = 3.25 \pm 0.49 \implies z_c \in [13.8 - 89.4]$ km
- $Q_2 = 3.58 \pm 0.36 \implies z_c > 11.9$ km
- $Q_3 = 3.81 \pm 0.29 \implies z_c > 14.9$ km

In the case considered here, no restriction can be further obtained on z_c from the Q-factor values (see figure 6b). Nevertheless, this example well illustrates the values of measuring several modes of the SR.

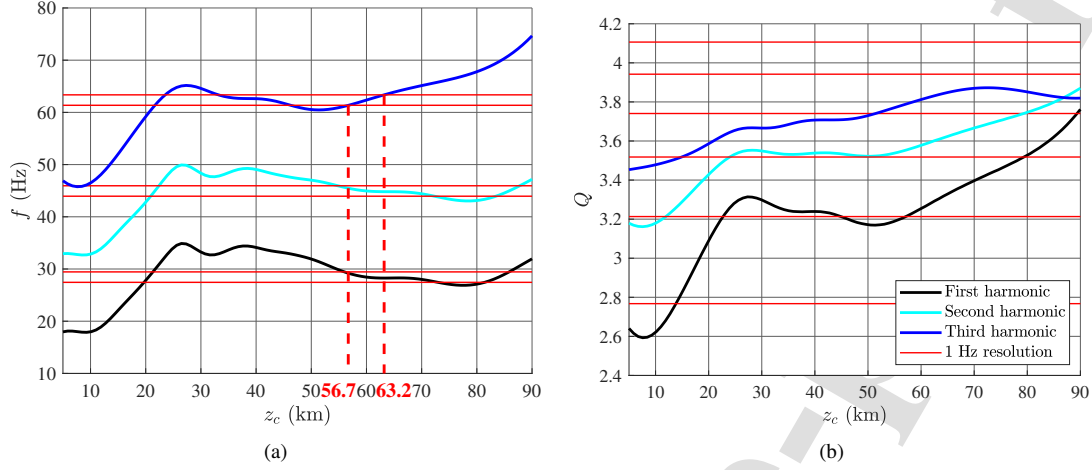


Figure 6: Variations of the resonant frequencies (f_1, f_2, f_3) (a) and of the quality factors (Q_1, Q_2, Q_3) (b) as a function of the thickness of the ice crust z_c assuming $\epsilon_c = 2.5, \sigma_c = 1.2 \text{ nS m}^{-1}$. The red lines embody the 1 Hz resolution and its corresponding quality factor resolution for the EFIELD measurement. In a case where the input value is $z_c = 60 \text{ km}$, the multi-modal analysis provides a range of values for z_c that is between 56.7 km and 63.2 km (dashed red lines)

4.3. Inversion uncertainty

259

260

261

262

263

264

265

266

267

The example above assumes fixed values for both ϵ_c and σ_c . To take into account our imperfect knowledge of the electrical properties of Titan's ice crust, the uncertainties on these parameters have to be propagated through the inversion to estimate their effects on the derivation of z_c . As another illustration, we numerically simulate Titan's cavity with a thickness of the ice crust fixed at $z_c = 60 \text{ km}$. A multi-modal analysis is then performed for every point ($z_c, \epsilon_c, \sigma_c$) in a regular parameter grid with ϵ_c and σ_c respectively varying in 2.5 ± 0.3 and $1.2 \pm 0.6 \text{ nS m}^{-1}$ as found at the Huygens landing site by Hamelin et al. (2016). The parameter grid consists of $17 \times 25 \times 25 = 15,300$ datapoints in the 3D parameter space $\{z_c\} \times \{\epsilon_c\} \times \{\sigma_c\}$. Every datapoint on the grid which returns the desired values for the first three modes considering their measurement uncertainty of 1 Hz is a possible inversion of EFIELD.

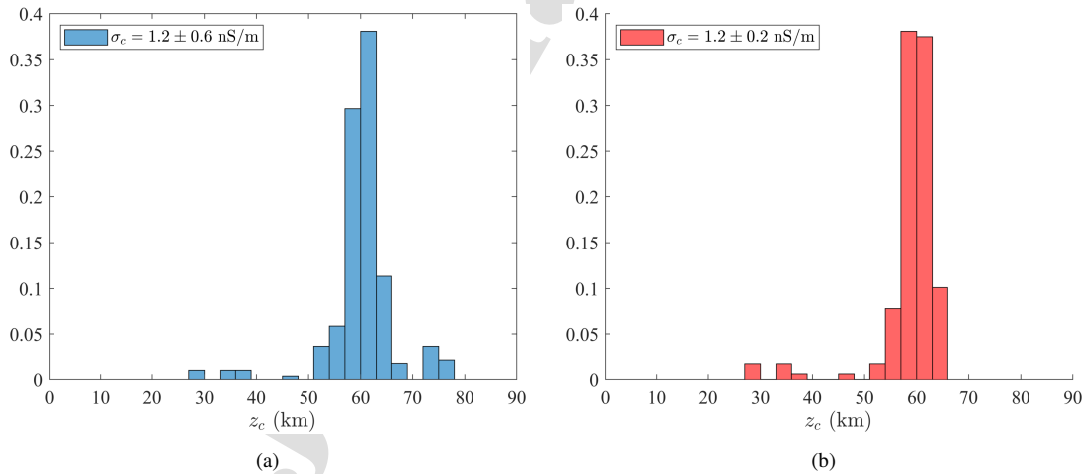


Figure 7: Relative frequencies histogram of the EFIELD inversion with 3 km intervals for an ice crust $z_c = 60 \text{ km}$ using the metamodelling process for two different uncertainties on σ_c : $\sigma_c = 1.2 \pm 0.6 \text{ nS m}^{-1}$ (a) and $\sigma_c = 1.2 \pm 0.2 \text{ nS m}^{-1}$ (b)

268 This allows us to compute the relative frequencies with 3 km intervals of the returned values of z_c assuming that
 269 the three first harmonic of the SR are detected with a resolution of 1 Hz, as figure 7a displays. Interestingly, 90%
 270 of the inversion cases fall in the range $z_c \in [51 - 69]$ km while $\approx 10\%$ of the cases return z_c values in the ranges
 271 $[20 - 40]$ km or $[70 - 80]$ km (blue bars). Assuming a normal distribution of z_c centered in 60 km, this corresponds to a
 272 standard deviation (STD) of 6.8 km. Figure 7b further shows that reducing the uncertainty on σ_c from $1.2 \pm 0.6 \text{ nS m}^{-1}$
 273 to $1.2 \pm 0.2 \text{ nS m}^{-1}$ reduces the STD to the value of 5.7 km.

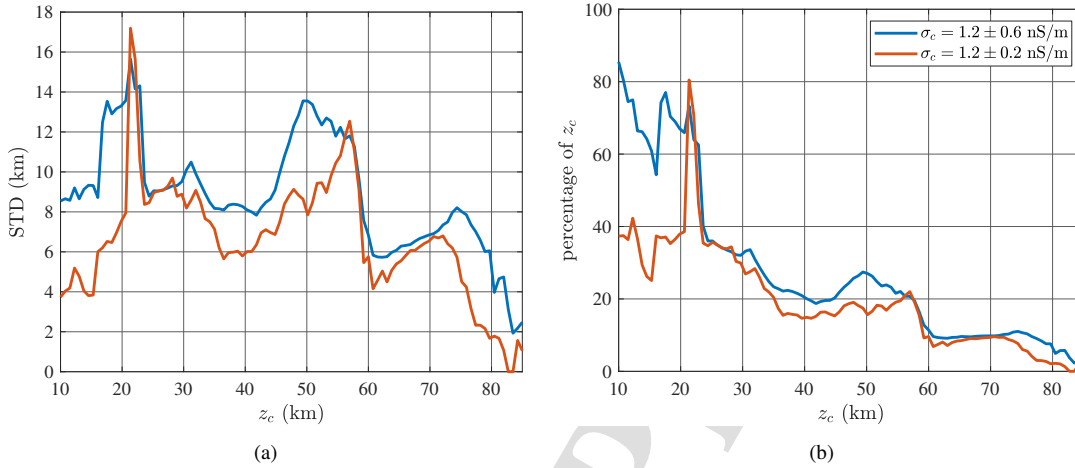


Figure 8: Standard deviation of the EFIELD inversion against the thickness of the ice crust z_c for two different uncertainties on σ_c in km (a) and percentage of z_c (b)

274 Such exercise was repeated for a set of z_c values in the $[10 - 85]$ km range to produce figure 8 which displays the
 275 STD (in km and %) of the distribution of the inferred z_c as a function of the z_c value for two assumptions on the range
 276 of variation of σ_c . In most cases, the STD is smaller than 10 km. Moreover, it significantly decreases as z_c increases,
 277 especially after 60 km where it becomes smaller than 10%. In contrast, for small values of z_c (< 25 km), the theoretical
 278 relative error on z_c can reach almost 100%. This can be partially explained by the relative coarse mesh of the numerical
 279 model; indeed the dimensions of the cells have been imposed greater than 5 km in order to reduce computation time.
 280 Further developments are required to build a surrogate model more appropriate to small thicknesses (i.e., with a finer
 281 mesh) but this is out of the scope of this paper.

282 The same analysis was conducted assuming a more constrained knowledge of σ_c (namely $\sigma_c = 1.2 \pm 0.2 \text{ nS m}^{-1}$)
 283 resulting in smaller STD for almost all cases (red lines in figure 8). In particular, the uncertainty at estimating small
 284 thicknesses drops from $\approx 80\%$ to $\approx 40\%$. This further shows the need for a more accurate knowledge of the electrical
 285 properties of the crust. This point and others are discussed in the following section.

286 5. Discussion and conclusion

287 For this work we have developed a numerical model of Titan's cavity to then build a less computationally expensive
 288 surrogate model able to describe how the cavity characteristics (i.e., eigenfrequency and Q-factors) vary with the main
 289 cavity parameters (i.e., Titan's ice crust thickness and electrical properties). This model (and its use for data inversion)
 290 is a powerful tool for the analysis of electric field measurements on Titan (and elsewhere). It was used to re-assess
 291 Huygens observations leading to the conclusion that the 2005 detection of a line at ~ 36 Hz, if indeed due to SR, does
 292 not provide any specific constraint on the depth of Titan's ocean in the range 5 – 200 km contrary to what is advanced
 293 in Béghin et al. (2012).

294 The surrogate model was also used to estimate the possible outcomes from the EFIELD/DraGMet/Dragonfly
 295 experiment. EFIELD is designed to detect several modes of SR with a fine spectral resolution; we have demonstrated
 296 that it has the ability to put a meaningful constraint on the thickness of the ice crust. Considering the electromagnetic
 297 properties varying in the ranges specified by Hamelin et al. (2016), the various sensitivity analysis presented throughout

298 this work, reach the same conclusion: although the thickness of the ice crust is the most influential parameter on SR
 299 characteristics, the resonant frequencies are dependent in the same order of magnitude on the electrical properties of
 300 Titan's crust. Therefore, in order to reduce the uncertainty at estimating Titan's crust thickness, it is crucial to reduce
 301 the uncertainty on the crust electrical properties.

302 Another experiment on board the Dragonfly drone will contribute to this task: the DIEL/DraGMet experiment.
 303 Acting as a mutual-impedance probe with a pair of electrodes mounted on each landing skid of the drone, DIEL will
 304 measure the complex permittivity (which includes the electrical conductivity) of the ground at several low frequencies
 305 (< 10 kHz) thus providing insights into the composition, moisture and porosity of the near-subsurface of Titan as
 306 well as on the spatial and temporal variations of such properties. Though all measured permittivity values may not
 307 be representative of the crust, values measured on the ejecta blanket of the geologically-young Selk crater (the final
 308 destination of Dragonfly) may be. In addition, variations of the measured complex permittivity along the Dragonfly
 309 journey to Selk and its possible correlation with otherwise inferred vicinity of the water ice bedrock in the near
 310 subsurface will provide further constraint on the ice crust electrical properties.

311 Nevertheless, as highlighted in Lorenz and Le Gall (2020), one of the main sources of uncertainty is and will remain
 312 our limited knowledge of the lower atmosphere conductivity structure. Unfortunately, no improvement is to be expected
 313 from forthcoming observations as Dragonfly will not perform measurements during its descent in Titan's atmosphere.
 314 As a consequence, only theoretical developments can provide further insights on the atmosphere conductivity profile
 315 and its expected variations with the local hour, solar activity and the position of Titan in Saturn's magnetosphere.

316 Future investigations will include the simulation of the actual EFIELD electrodes accommodated on the Dragonfly
 317 (conductive) body as well as the study of the effect on measurements of the location and polarization of the possible
 318 sources of SR. In the mid-2030s, when the Dragonfly drone will be on Titan, methane-storms are expected at the
 319 South Pole. Though still speculative, such storms might be associated with some atmospheric electric phenomena
 320 which could generate SRs that the EFIELD experiment (located at much lower latitudes) will try to detect. Given the
 321 different orientation and altitude on the drone of the two EFIELD electrodes, at least two components of the electrical
 322 field will be measured. The third component could be captured by rotating the drone and future study will also explore
 323 the value of measuring the full electrical field vector.

324 Lastly, the approach we have developed in this paper, based on the development and use of a surrogate model, can
 325 be readily applied to the study of SR in other bodies in the Solar System such as Venus. In particular it may help better
 326 characterize the electrical environment of Venus by comparison to Venera 11 and 12 past observations or DaVinci
 327 future electric measurements, if any.

328 Acknowledgements

329 The authors wish to thank Ralph Lorenz (APL, PI of DraGMet/Dragonfly) and Jean-Jacques Berthelier, Audrey
 330 Chatain and Franck Montmessin from LATMOS for useful discussions on this project. The authors are also grateful
 331 to Région Ile-de-France (DIM-ACAV+ program) for funding this research.

332 References

- 333 Baland, R.M., Tobie, G., Lefèvre, A., Van Hoolst, T., 2014. Titan's internal structure inferred from its gravity field, shape, and rotation state. *Icarus*
 334 237, 29–41.
- 335 Baland, R.M., Van Hoolst, T., Yseboodt, M., Karatekin, Ö., 2011. Titan's obliquity as evidence of a subsurface ocean? *Astronomy & Astrophysics*
 336 530, A141.
- 337 Barnes, J.W., Turtle, E.P., Trainer, M.G., Lorenz, R.D., MacKenzie, S.M., Brinckerhoff, W.B., Cable, M.L., Ernst, C.M., Freissinet, C., Hand, K.P.,
 338 et al., 2021. Science goals and objectives for the dragonfly titan rotorcraft relocatable lander. *The Planetary Science Journal* 2, 130.
- 339 Béghin, C., Randriamboarison, O., Hamelin, M., Karkoschka, E., Sotin, C., Whitten, R.C., Berthelier, J.J., Grard, R., Simões, F., 2012. Analytic
 340 theory of titan's schumann resonance: Constraints on ionospheric conductivity and buried water ocean. *Icarus* 218, 1028–1042.
- 341 Béghin, C., Simões, F., Krasnoselskikh, V., Schwingenschuh, K., Berthelier, J.J., Besser, B., Bettanini, C., Grard, R., Hamelin, M., López-Moreno,
 342 J., et al., 2007. A schumann-like resonance on titan driven by saturn's magnetosphere possibly revealed by the Huygens probe. *Icarus* 191,
 343 251–266.
- 344 Bills, B.G., Nimmo, F., 2008. Forced obliquity and moments of inertia of titan. *Icarus* 196, 293–297.
- 345 Bills, B.G., Nimmo, F., 2011. Rotational dynamics and internal structure of titan. *Icarus* 214, 351–355.
- 346 Chatain, A., Le Gall, A., Berthelier, J.J., Lorenz, R.D., Hassen-Khodja, R., Lebret, J.P., Joly-Jehenne, T., Déprez, G., 2023. Detection and
 347 characterization of wind-blown charged sand grains on titan with the dragmet/efield experiment on dragonfly. *Icarus* 391, 115345.
- 348 Durante, D., Hemingway, D., Racioppa, P., Iess, L., Stevenson, D., 2019. Titan's gravity field and interior structure after cassini. *Icarus* 326,
 349 123–132.

- 350 Elisseeff, A., Pontil, M., et al., 2003. Leave-one-out error and stability of learning algorithms with applications. *NATO science series sub series iii*
 351 *computer and systems sciences* 190, 111–130.
- 352 Fischer, G., Farrell, W., Gurnett, D., Kurth, W., 2020. Nondetection of radio emissions from titan lightning by cassini rpws. *Journal of Geophysical*
 353 *Research: Planets* 125, e2020JE006496.
- 354 Fischer, G., Gurnett, D., 2011. The search for titan lightning radio emissions. *Geophysical research letters* 38.
- 355 Fischer, G., Gurnett, D.A., Kurth, W.S., Farrell, W.M., Kaiser, M.L., Zarka, P., 2007. Nondetection of titan lightning radio emissions with
 356 cassini/rpws after 35 close titan flybys. *Geophysical research letters* 34.
- 357 Fulchignoni, M., Ferri, F., Angrilli, F., Ball, A., Bar-Nun, A., Barucci, M., Bettanini, C., Bianchini, G., Borucki, W., Colombatti, G., et al., 2005.
 358 In situ measurements of the physical characteristics of titan's environment. *Nature* 438, 785–791.
- 359 Goossens, S., van Noort, B., Mateo, A., Mazarico, E., van der Wal, W., 2024. A low-density ocean inside titan inferred from cassini data. *Nature*
 360 *Astronomy*, 1–10.
- 361 Grard, R., Hamelin, M., López-Moreno, J., Schwingenschuh, K., Jernej, I., Molina-Cuberos, G., Simões, F., Trautner, R., Falkner, P., Ferri, F., et al.,
 362 2006. Electric properties and related physical characteristics of the atmosphere and surface of titan. *Planetary and Space Science* 54, 1124–1136.
- 363 Hamelin, M., Grard, R., López-Moreno, J., Schwingenschuh, K., Béghin, C., Berthelier, J., Simões, F., 2009. Comment on "evidence of electrical
 364 activity on titan drawn from the schumann resonances sent by Huygens probe" by j.a. morente, j.a. portí, a. salinas, e.a. navarro [2008,
 365 *icarus*, 195, 802–811]. *Icarus* 204, 349–351. URL: <https://www.sciencedirect.com/science/article/pii/S0019103509000748>,
 366 doi:<https://doi.org/10.1016/j.icarus.2009.01.031>.
- 367 Hamelin, M., Lethuillier, A., Le Gall, A., Grard, R., Schwingenschuh, K., Jernej, I., López-Moreno, J.J., Brown, V., Lorenz, R.D., et al.,
 368 2016. The electrical properties of titan's surface at the Huygens landing site measured with the pwa-hasi mutual impedance probe. new approach
 369 and new findings. *Icarus* 270, 272–290.
- 370 Iess, L., Jacobson, R.A., Ducci, M., Stevenson, D.J., Lunine, J.I., Armstrong, J.W., Asmar, S.W., Racioppa, P., Rappaport, N.J., Tortora, P., 2012.
 371 The tides of titan. *Science* 337, 457–459.
- 372 Kronrod, V., Dunaeva, A., Gudkova, T., Kuskov, O., 2020. Matching of models of the internal structure and thermal regime of partially differentiated
 373 titan with gravity field. *Solar System Research* 54, 405–419.
- 374 Lagouanelle, P., Freschi, F., Pichon, L., 2023. Adaptive sampling for fast and accurate metamodel-based sensitivity analysis of complex
 375 electromagnetic problems. *IEEE Transactions on Electromagnetic Compatibility*.
- 376 Lorenz, R., 1997. Lightning and triboelectric charging hazard assessment for the Huygens probe, in: *Huygens: Science, Payload and Mission*,
 377 *Proceedings of an ESA conference*. Edited by A. Wilson (1997), p. 265, p. 265.
- 378 Lorenz, R.D., 2021. The low electrical conductivity of titan's lower atmosphere. *Icarus* 354, 114092.
- 379 Lorenz, R.D., Le Gall, A., 2020. Schumann resonance on titan: A critical re-assessment. *Icarus* 351, 113942.
- 380 Lorenz, R.D., Turtle, E.P., Barnes, J.W., Trainer, M.G., Adams, D.S., Hibbard, K.E., Sheldon, C.Z., Zacny, K., Peplowski, P.N., Lawrence, D.J.,
 381 et al., 2018. Dragonfly: A rotorcraft lander concept for scientific exploration at titan. *Johns Hopkins APL Technical Digest* 34, 14.
- 382 Marelli, S., Sudret, B., 2014. UQLab: A framework for uncertainty quantification in Matlab. *American Society of Civil Engineers*.
- 383 Mattei, E., Lauro, S., Vannaroni, G., Cosciotti, B., Bella, F., Pettinelli, E., 2014. Dielectric measurements and radar attenuation estimation of
 384 ice/basalt sand mixtures as martian polar caps analogues. *Icarus* 229, 428–433.
- 385 Meriggiola, R., Iess, L., Stiles, B.W., Lunine, J.I., Mitri, G., 2016. The rotational dynamics of titan from cassini radar images. *Icarus* 275, 183–192.
- 386 Schobi, R., Sudret, B., Wiart, J., 2015. Polynomial-chaos-based kriging. *International Journal for Uncertainty Quantification* 5.
- 387 Schumann, W.O., 1952. Über die strahlungslosen eigenschwingungen einer leitenden kugel, die von einer luftschicht und einer ionosphärenhülle
 388 umgeben ist. *Zeitschrift für Naturforschung A* 7, 149–154.
- 389 Simoes, F., 2007. Theoretical and experimental studies of electromagnetic resonances in the ionospheric cavities of planets and satellites; instrument
 390 and mission perspectives. Ph.D. thesis. Université Pierre et Marie Curie-Paris VI.
- 391 Simões, F., Grard, R., Hamelin, M., López-Moreno, J., Schwingenschuh, K., Béghin, C., Berthelier, J.J., Besser, B., Brown, V., Chabassière, M.,
 392 et al., 2007. A new numerical model for the simulation of ELF wave propagation and the computation of eigenmodes in the atmosphere of titan:
 393 Did Huygens observe any Schumann resonance? *Planetary and Space Science* 55, 1978–1989.
- 394 Simões, F., Grard, R., Hamelin, M., López-Moreno, J., Schwingenschuh, K., Béghin, C., Berthelier, J.J., Lebreton, J.P., Molina-Cuberos, G., Tokano,
 395 T., 2008a. The Schumann resonance: A tool for exploring the atmospheric environment and the subsurface of the planets and their satellites.
 396 *Icarus* 194, 30–41.
- 397 Simões, F., Hamelin, M., Grard, R., Aplin, K., Béghin, C., Berthelier, J.J., Besser, B., Lebreton, J.P., López-Moreno, J., Molina-Cuberos, G., et al.,
 398 2008b. Electromagnetic wave propagation in the surface-ionosphere cavity of Venus. *Journal of Geophysical Research: Planets* 113.
- 399 Sobol, I.M., 1993. Sensitivity analysis for non-linear mathematical models. *Mathematical modelling and computational experiment* 1, 407–414.
- 400 Stiles, B.W., Kirk, R.L., Lorenz, R.D., Hensley, S., Lee, E., Ostro, S.J., Allison, M.D., Callahan, P.S., Gim, Y., Iess, L., et al., 2008. Determining
 401 titan's spin state from Cassini radar images. *The Astronomical Journal* 135, 1669.
- 402 Turtle, E., Barnes, J., Trainer, M., Lorenz, R., Hibbard, K., Adams, D., Bedini, P., Brinckerhoff, W., Cable, M., Ernst, C., et al., 2018. Dragonfly:
 403 In situ exploration of titan's organic chemistry and habitability, in: 49th lunar and planetary science conference, pp. LPI-Contribution.
- 404 Van Steenkiste, T., van der Herten, J., Couckuyt, I., Dhaene, T., 2016. Sensitivity analysis of expensive black-box systems using metamodeling, in:
 405 2016 Winter Simulation Conference (WSC), IEEE, pp. 578–589.
- 406 Zimmerman, W.B., 2006. Multiphysics modeling with finite element methods. volume 18. World Scientific Publishing Company.

Declaration of interests

The authors declare that they have no known competing financial interests or personal relationships that could have appeared to influence the work reported in this paper.

The authors declare the following financial interests/personal relationships which may be considered as potential competing interests:

Journal Pre-proof